



Cite this: DOI: 10.1039/c6ob00993j

Catalytic signal amplification for the discrimination of ATP and ADP using functionalised gold nanoparticles†

Cristian Pezzato, Jack L.-Y. Chen, Patrizia Galzerano, Michela Salvi and Leonard J. Prins*

Diagnostic assays that incorporate a signal amplification mechanism permit the detection of analytes with enhanced selectivity. Herein, we report a gold nanoparticle-based chemical system able to differentiate ATP from ADP by means of catalytic signal amplification. The discrimination between ATP and ADP is of relevance for the development of universal assays for the detection of enzymes which consume ATP. For example, protein kinases are a class of enzymes critical for the regulation of cellular functions, and act to modulate the activity of other proteins by transphosphorylation, transferring a phosphate group from ATP to give ADP as a byproduct. The system described here exploits the ability of cooperative catalytic head groups on gold nanoparticles to very efficiently catalyze chromogenic reactions such as the transphosphorylation of 2-hydroxypropyl-4-nitrophenyl phosphate (HPNPP). A series of chromogenic substrates have been synthesized and evaluated by means of Michaelis-Menten kinetics (compounds **2**, **4–6**). 2-Hydroxypropyl-(3-trifluoromethyl-4-nitro)phenyl phosphate (**5**) was found to display higher reactivity (k_{cat}) and higher binding affinity (K_M) when compared to HPNPP. This higher binding affinity allows phosphate **5** to compete with ATP and ADP to different extents for binding on the monolayer surface, thus enabling a catalytically amplified signal only when ATP is absent. Overall, this represents a viable new approach for monitoring the conversion of ATP into ADP with high sensitivity.

Received 6th May 2016,
Accepted 16th June 2016
DOI: 10.1039/c6ob00993j

www.rsc.org/obc

Introduction

The detection of low levels of proteins and other biomarkers is of crucial importance for the early diagnosis of diseases.^{1–3} In particular, the development of technology that allows naked eye detection of target molecules without the need for complex instrumentation is the utmost challenge.⁴ In particular, assays that allow for the detection of ATP consumption are important as ATP is used as a source of energy for numerous biochemical processes. For example, protein kinases are a class of enzymes that play critical roles in a variety of cellular functions including cell growth, development, differentiation, membrane transport, and cell death.^{5–8} They exert their function by transferring the γ -phosphate group of ATP to a serine, threonine or tyrosine residue in specific substrate proteins (forming ADP as a by-product), which are crucially involved in multiple signaling pathways within the body. Thus the ability to differentiate ADP from ATP could provide a universal assay for

protein kinases as well as other enzymes which involve ATP consumption.

Assays for ATP consumption traditionally rely on the use of ³²P-labeled ATP to ensure high sensitivity.⁹ However, this comes with disadvantages such as the short life-time of ³²P-labelled ATP and the generation of radioactive waste. These traditional protocols are also laborious and non-conducive to high-throughput screening. Due to these limitations, there has been much research towards non-radioactive assays for ATP consumption,¹⁰ with particular emphasis on techniques based on fluorescence.^{11–16} While exciting, many of these alternative methodologies rely on elaborate constructs involving fluorophores conjugated to enzymes or antibodies. More recent work has emphasised the need for novel methodologies that rely on less-complex elements.^{17–24} Herein, we present novel methodology using simple and robust components able to visually discriminate ATP and ADP at low concentrations by means of catalytic signal amplification.

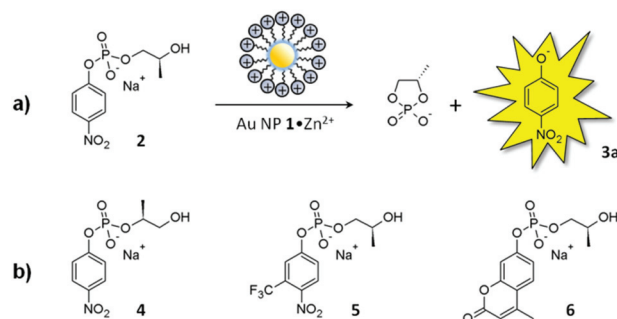
The focus here is on the use of catalytic signal amplification.²⁵ This allows for highly sensitive assays where a single analyte molecule triggers the activation of a signal amplification pathway which leads to the generation of a large number of reporter molecules.⁴ This marks a strong contrast with con-

Department of Chemical Sciences, University of Padova, Via Marzolo 1, 35131 Padova, Italy. E-mail: leonard.prins@unipd.it

†Electronic supplementary information (ESI) available. See DOI: 10.1039/c6ob00993j

ventional chemosensing assays in which a fixed correlation exists between the amount of analyte and the output signal. Signal amplification mechanisms typically rely on the use of multivalent systems or catalysts,^{25–29} in which the analyte affects the properties of a multitude of reporter molecules or activates an (auto)catalytic pathway. Recently, we developed a catalytic signal amplification assay for the detection of protease activity that relied on the use of gold nanoparticles (Au NP 1, Fig. 1) passivated with a monolayer of thiols terminating with 1,4,7-triazacyclonane (TACN)·Zn²⁺ head groups.^{30,31}

This system catalyses very efficiently the transphosphorylation of 2-hydroxypropyl-4-nitrophenylphosphate (HPNPP 2; Scheme 1a), a model substrate for RNA hydrolysis,^{32–38} due to the cooperative action between neighbouring TACN·Zn²⁺ head groups in the monolayer.^{39,40} This reaction liberates *p*-nitrophenol (3a), which is easily detectable by the naked eye. In addition, negatively charged oligoanions such as peptides and nucleotides (*e.g.* ATP and ADP) have been found to have very high affinity for the surface of nanoparticles because of the high density of positive charges in the monolayer.^{41–45} A strong correlation between the binding affinity and the number of charges present in the oligoanions was observed.⁴⁶ Importantly, the binding of negatively charged oligoanions to the surface of Au NP 1 blocks the binding sites for the substrate HPNPP 2, thus inhibiting catalysis. The working principle of our previous assay for protease activity relied on the use of negatively charged peptides which acted both as (1) substrates of the target proteases and (2) as inhibitors of the HPNPP cleavage activity of the gold nanoparticles. Cleavage of the substrates by proteases resulted in fragments with less overall negative charge, thus possessing lower inhibitory power for the gold nanoparticles, causing a turn on of catalytic activity (HPNPP hydrolysis) and the formation of reporter molecules (3a). It was shown that the selectivity of the assay towards different enzyme targets could be tuned by changing the peptide sequence. However, this system was not able to differentiate ATP and ADP because ATP and ADP both had such high affinities for the gold nanoparticles compared to



Scheme 1 (a) Transphosphorylation of HPNPP 2 catalysed by Au NP 1 to form a cyclic organic phosphate with the release of *p*-nitrophenol 3a; (b) the different analogues of HPNPP investigated in this work.

HPNPP that both bound under saturation conditions (as in the lower hemisphere of Fig. 1). Consequently, ATP → ADP conversion never resulted in reactivation of the catalytic activity (as in the upper hemisphere of Fig. 1). This is regrettable, because the ability to detect ATP → ADP conversion would provide access to a universal assay for the detection of protein kinases using catalytic signal amplification.

Here, we were interested to investigate whether this supramolecular approach could be customized to allow for the discrimination of ATP and ADP. As mentioned above, the addition of either ATP or ADP to a system containing Au NP 1 and HPNPP 2 caused an immediate and quantitative inhibition of catalytic activity. This implies that the affinity of the substrate HPNPP 2 for Au NP 1 was just too weak when compared to ADP. What is required is an HPNPP analogue with a higher affinity for Au NP 1, strong enough to displace ADP, but not ATP. Recent studies by us and others have demonstrated that the binding of small molecules on the monolayer depends on a combination of noncovalent interactions, including hydrophobic ones.^{47–53} Thus, we reasoned that by modifying the chemical structure of HPNPP 2 it could be possible to make a new substrate with a higher affinity (K_M) for Au NP 1.

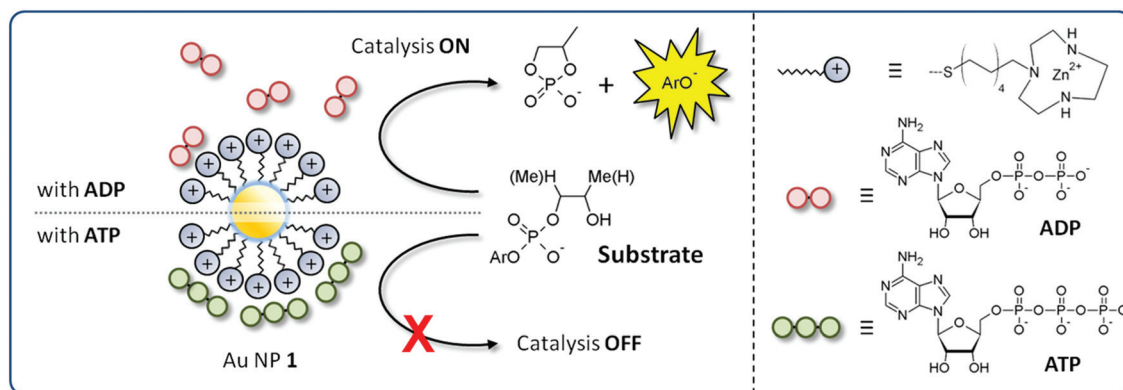


Fig. 1 The lower hemisphere shows ATP binding to the surface of Au NP 1, which blocks the catalytic sites (TACN headgroups) and inhibits the catalytic conversion of the substrate to the chromogenic reporter molecule. The upper hemisphere shows the lower binding affinity of ADP, which allows the catalytic conversion of the substrate to a chromogenic product.

This would lead to more effective (and different) competition with ATP and ADP for binding with the NP surface, thus enabling their discrimination. In addition, an improvement in the reactivity of the substrate (k_{cat}) and/or chromogenic properties (molar extinction coefficient) would permit an improvement in terms of the signal output by the catalytic assay and, thus, its sensitivity.

Results and discussion

Substrate analysis

Two different approaches have been taken for the structural modification of HPNPP (2), acting either on the internal nucleophile or the chromogenic leaving group (Scheme 1b). The first approach involves a change in the nucleophilicity of the hydroxyl group by switching from a secondary to a primary hydroxyl group (compound 4). This was expected to favourably affect the cyclization rate because of reduced steric hindrance. Secondly, changes in the structure of the leaving group (compounds 5 and 6) can be used to affect features such as reactivity, substrate polarity (with an effect on K_M) and signal strength (molar absorption coefficient). After examination of a series of potential candidates, we decided to examine two

leaving groups in more detail (Fig. 2). 3-Trifluoromethyl-4-nitrophenol (**3b**) possesses several interesting features: the presence of a trifluoromethyl group in position 3 of the phenol ring decreases the acidity of the leaving group with respect to **3a** (pK_a from 7.15 to 6.07),⁵⁴ while also ensuring a higher hydrophobic contribution to the overall molecular structure. This substrate was thus expected to exhibit enhanced binding affinity to the nanoparticle surface. On the other hand, despite the fact that 4-methylumbelliferone (**3c**) possesses a higher pK_a (7.79),⁵⁵ we were attracted by this leaving group because of its fluorescence properties, which would in principle provide a significant increase in sensitivity. In this context, it is worth noting how the pK_a of phenols determine their optical properties. In general, phenols show two characteristic absorption bands in water. The band at shorter wavelengths originates from the protonated form while the band at longer wavelengths is associated to the deprotonated form. At a given pH, the equilibrium between the two forms is dependent on the pK_a value. In order to quantify how the acidity of the leaving group influences the optical properties of chromophores **3a–c**, we recorded the UV-Vis spectra as a function of the pH (from pH 6.0 to 8.0, Fig. 2).

It can be observed that an increase in the pH causes an increase in the absorption band originating from the deproto-

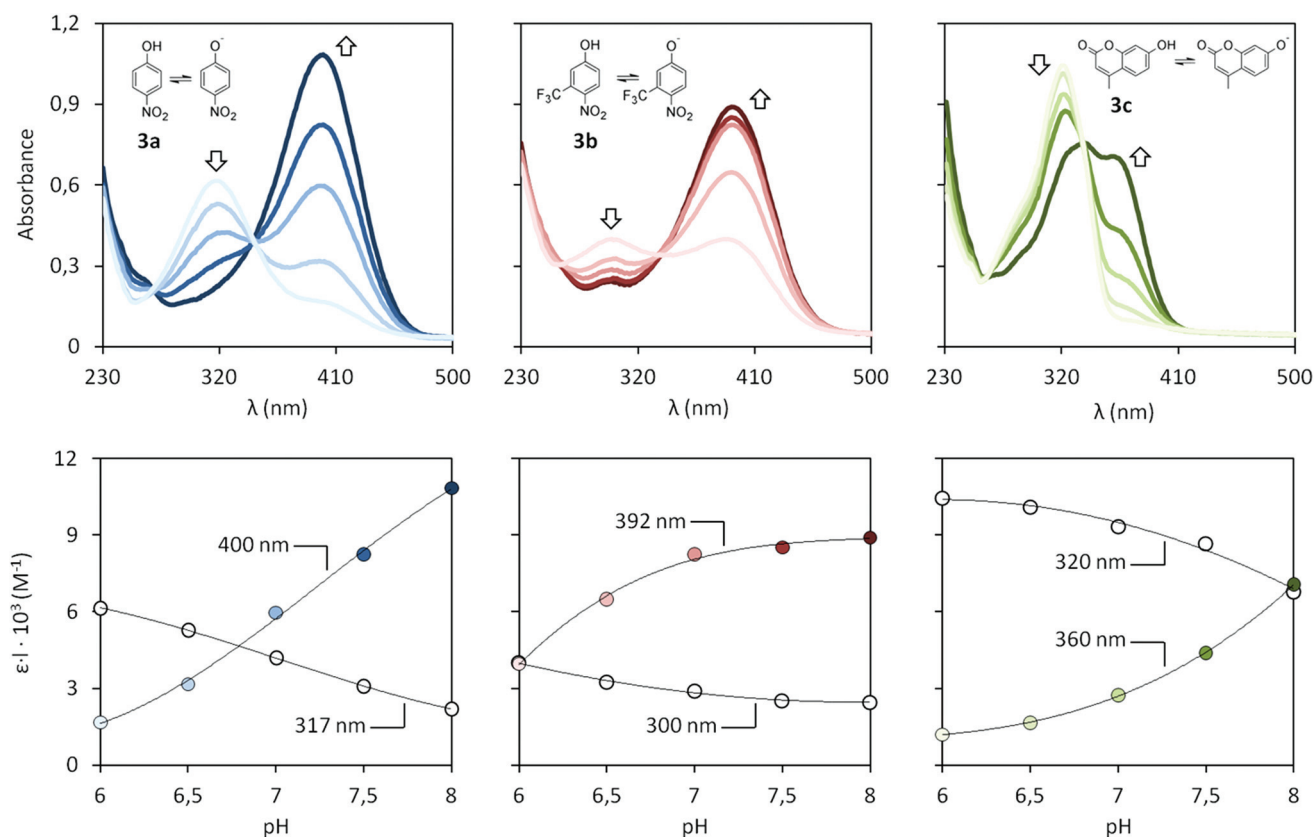
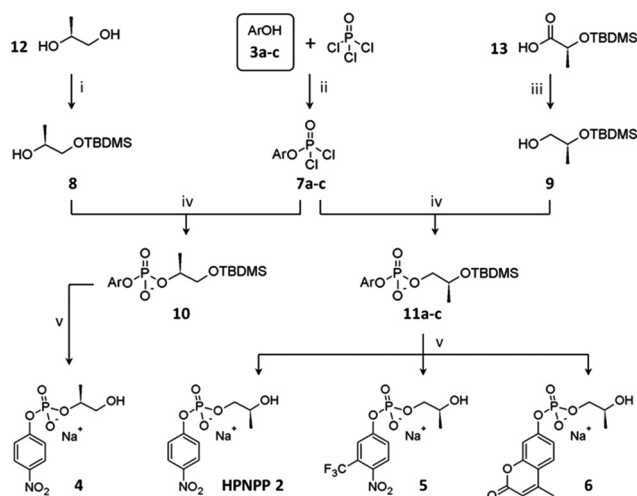


Fig. 2 UV-Vis spectra of chromophores **3a–c** as a function of pH (arrows show increase in pH). The behaviour of the corresponding molar absorption coefficients as a function of the pH is reported on the bottom. To account for the inaccuracy of measuring the optical path length in a microtiter well we decided to report $\epsilon \cdot l$. Experimental conditions: [**3a**] = [**3b**] = [**3c**] = 100 μM , [MES] = 10 mM, pH = 6.0 and 6.5, [HEPES] = 10 mM, pH = 7.0, 7.5 and 8.0, 40 $^{\circ}C$.

nated form ($\lambda_{\max} = 400$ nm for **3a**, 392 nm for **3b** and 360 nm for **3c**). The trends of the molar absorptivity as a function of pH are in line with the corresponding pK_a 's. In particular, **3b** displayed the best response up to pH 7.5, which illustrates the important advantage of using more acidic reporter molecules like **3b** at physiological pH's. Although the protonated forms also have significant absorptivities at lower pH values (in particular **3c**), from a practical point of view the absorption band originating from the protonated form is often less useful for signal generation, because of the frequent presence of other chromophores that also absorb at lower wavelengths.

Substrate synthesis

Based on this initial analysis, three substrates for Au NP **1** have been synthesized according to Scheme 2. Substrate **4** is an analogue of HPNPP (**2**) but contains a primary hydroxyl group rather than a secondary one. Substrates **5**⁵⁸ and **6** are analogues containing leaving groups **3b** and **3c**, respectively. The key intermediate in all these syntheses is an aryl phosphorodichloridate (**7a-c**),⁵⁷ which was synthesized by slowly adding pyridine to a solution of phosphorus oxychloride and the corresponding phenol (**3a-c**) in dry toluene. Coupling of phosphorodichloridates **7a-c** with monoprotected diol **8** or **9** in dry THF with triethylamine as base furnished the corresponding precursors **10** and **11a-c** as triethylammonium salts with moderate to good yield.⁵⁶ Compound **8** was obtained by the silyl mono-protection of commercially available (*S*)-(+)-1,2-propanediol (**12**), while compound **9** was synthesized by reducing commercially available ethyl (*S*)-(-)-2-(*tert*-butyldimethylsilyloxy)propionate (**13**) with $BH_3 \cdot THF$.⁵⁶



Scheme 2 General synthesis of HPNPP analogues.^{56,57} Reaction conditions: (i) TBDMSCl (dropwise at 0 °C), imidazole, DCM, RT for 2 h (78%); (ii) pyridine (dropwise at 95 °C), toluene, 110 °C for 15 min; (iii) $BH_3 \cdot THF$ (dropwise at 0 °C), THF, 66 °C for 5 h (87%); (iv) **8** or **9** (dropwise at 0 °C), **7a-c**, THF, RT for 2–5 h (40–90%); (v) **10** or **11a-c** TEA·3HF, THF, 0 °C to RT, overnight; Na^+ ion exchange, prep. rev. phase HPLC (25–30%).

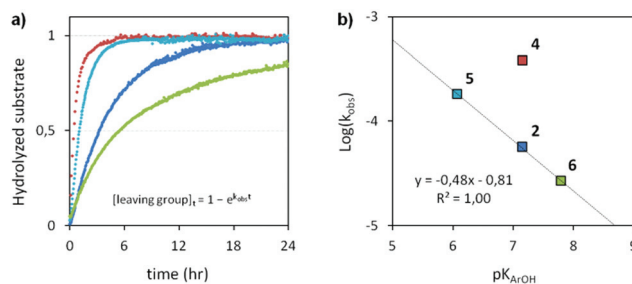


Fig. 3 Alkaline hydrolysis study. Experimental conditions: [substrate] = 50 μ M, [CAPS] = 10 mM, pH = 11.0, 40 °C. See ESI† for more details.

Finally, all the precursors were deprotected using triethylamine·3HF and passed through a SP-Sephadex column (Na^+ form). All substrates **2** and **4–6** were obtained as sodium salts with moderate yields after preparative reverse phase HPLC.

Intrinsic substrate reactivity

The intrinsic reactivity of the new substrates was first evaluated by observing their base-induced hydrolysis kinetics at pH 11. Substrates were incubated at 40 °C and the reaction was monitored following the absorbance of the corresponding leaving group (Fig. 3a). In all cases, the experimental profiles could be fitted to a first order kinetic model ($R^2 > 95$). The obtained pseudo-first order constants (k_{obs}) could be directly related to the molecular structure of the substrates. This was clearly seen from an analysis of the Brønsted plot (Fig. 3b), in which $\log k_{obs}$ is plotted against the pK_a of the corresponding leaving group (pK_{ArOH}). For substrates **2**, **5** and **6** a clear linear correlation was observed between the $\log k_{obs}$ and pK_{ArOH} , supporting a mechanism in which the dissociation of the leaving group is the rate-determining step. In addition, quantitative analysis revealed that substrate **5** is 3 times more reactive than **2**, which, in turn, is 2 times more reactive than substrate **6**. The importance of having a better internal nucleophile is reflected by the behavior of substrate **4**, which is hydrolyzed 7 times faster than **2**.

We next investigated the effect of structural changes in the substrate on the catalytic properties of Au NP **1**. Kinetic measurements were carried out at three different pHs (6.0, 7.0 and 8.0) by monitoring the rate of formation of leaving groups **3a-c** as a function of the concentration of substrates **2** and **4–6**. At each pH, a calibration curve was used to convert the measured absorbance originating from **3a-c** into the corresponding initial rate (see ESI†). Plots of the obtained initial reaction rates as a function of substrate concentration demonstrate that all substrates are cleaved by Au NP **1** obeying Michaelis-Menten-like enzyme kinetics (Fig. 4). Accordingly, all curves were fitted to the Michaelis-Menten model yielding the parameters k_{cat} and K_M as listed in Table 1.

The purpose of this study was the identification of improved alternative substrates to HPNPP **2**, both in terms of reactivity (k_{cat}) and binding affinity (K_M), with the aim of improving both the efficacy of signal generation in a catalytic

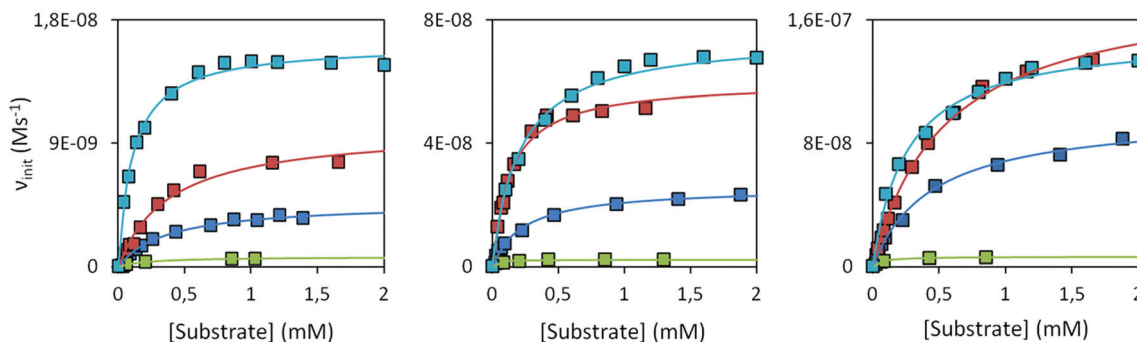


Fig. 4 Initial rates for the cleavage of **2** (dark blue), **4** (red), **5** (light blue) and **6** (green) by Au NP **1** at three different pHs. Experimental conditions: $[\text{TACN-Zn}^{2+}] = 20 \pm 1 \mu\text{M}$, $[\text{substrate}] = 0\text{--}2.0 \text{ mM}$, $[\text{HEPES}] = 10 \text{ mM}$, $\text{pH} = 7.0$ and 8.0 , $[\text{MES}] = 10 \text{ mM}$, $\text{pH} 6.0$, $40 \text{ }^\circ\text{C}$.

Table 1 Michaelis-Menten parameters obtained for substrate **2** and **4–6**

| Substrate | pH 6.0 | | pH 7.0 | | pH 8.0 | |
|------------------|--|----------------------------|--|----------------------------|--|----------------------------|
| | $k_{\text{cat}} [\times 10^{-3} \text{ s}^{-1}]$ | $k_{\text{m}} [\text{mM}]$ | $k_{\text{cat}} [\times 10^{-3} \text{ s}^{-1}]$ | $k_{\text{m}} [\text{mM}]$ | $k_{\text{cat}} [\times 10^{-3} \text{ s}^{-1}]$ | $k_{\text{m}} [\text{mM}]$ |
| 2 (HPNPP) | 0.2 ± 0.03 | 0.4 ± 0.05 | 1.4 ± 0.1 | 0.3 ± 0.04 | 4.9 ± 0.2 | 0.5 ± 0.03 |
| 4 | 0.5 ± 0.05 | 0.4 ± 0.05 | 3.0 ± 0.2 | 0.1 ± 0.02 | 9.2 ± 0.2 | 0.5 ± 0.03 |
| 5 | 0.8 ± 0.1 | 0.1 ± 0.03 | 3.8 ± 0.2 | 0.2 ± 0.02 | 7.6 ± 0.2 | 0.3 ± 0.02 |
| 6 | 0.04 ± 0.01 | 0.3 ± 0.05 | 0.1 ± 0.05 | 0.04 ± 0.01 | 0.3 ± 0.04 | 0.07 ± 0.01 |

signal amplification assay and the possibility to differentiate between ATP and ADP. Upon examining the Michaelis-Menten curves in Fig. 4, it can be seen that the observed k_{cat} for **4**, the substrate with the primary internal nucleophile, was two times higher than for HPNPP over the entire pH range tested. While this was exciting in terms of reactivity and the potential responsiveness of the system, the exhibited K_{M} values were very close to those of HPNPP, which suggested that this substrate was unlikely to exhibit enhanced affinity for the NPs to compete with the binding of ADP.

The fluorogenic substrate **6**, on the other hand, showed K_{M} values much lower than that observed for HPNPP (at pH's 7 and 8). This shows that substrate **6** should exhibit significantly higher affinity for Au NP **1** than HPNPP, which would facilitate the discrimination between ATP and ADP. Unfortunately, substrate **6** was also dramatically less reactive than HPNPP (up to 15 times at pH 8.0), which rendered the substrate ineffective for a catalytic amplification assay.

Finally, we were pleased to observe that CF_3 -substituted substrate **5** showed very promising properties, both in terms of k_{cat} and K_{M} . Substrate **5** was observed to be up to 3 times more reactive than HPNPP over the entire range of pH studied and showed unprecedented high affinity at pH 6.0 ($K_{\text{M}} = 0.11 \text{ mM}$). This lower K_{M} is due likely to the increased hydrophobic contribution from the CF_3 group, which should increase binding affinity to the monolayer of the Au NPs. However, a general analysis of the K_{M} -values measured for all compounds indicate that hydrophobic interactions alone do not account for the stability of the interaction with Au NP **1**. If that would have been the case, a lower dependence of the K_{M} -values on the pH

would have been observed. Altogether it indicates that the interaction between small molecules and the organic monolayer is governed by a combination of noncovalent interactions, which is in line with previous observations made by us and others.^{47,48,51,53} In light of these observations, together with its improved absorptivity (see Fig. 1), we decided that substrate **5** was the best candidate for pursuing improvements in the catalytic signal amplification assay both in terms of sensitivity and applicability.

ATP/ADP-inhibition and signal amplification studies

The key hypothesis of this study was that a substrate (like compound **5**) with a higher affinity for Au NP **1** than HPNPP (**2**) would be able to compete more efficiently with ATP and ADP for binding to the monolayer of the Au NPs. This idea was tested by performing a series of inhibition experiments in which the cleavage of **5** by Au NP **1** was inhibited with increasing amounts of ATP or ADP (Fig. 5). Substrate **5** was added to give an initial concentration of 1 mM and the release of chromophore **3b** was measured by monitoring the increase in absorbance at 392 nm. The obtained initial reaction rates ($\nu_{\text{init},1}$) were normalized over the initial rate in the absence of inhibitor ($\nu_{\text{init},0}$) and were plotted as a function of the concentration of inhibitor added. As for the Michaelis-Menten kinetics, the inhibition experiments were repeated at three different pHs (6.0, 7.0 and 8.0, Fig. 5a–c). We were very pleased to observe that in all cases, ATP and ADP inhibited the catalysis of HPNPP to different extents, with a maximum difference at a concentration of inhibitors equal to $6.4 \mu\text{M}$ (see the yellow rectangles). The ratio of the relative initial rates ($\nu_{\text{ADP}}/\nu_{\text{ATP}}$) (*i.e.*

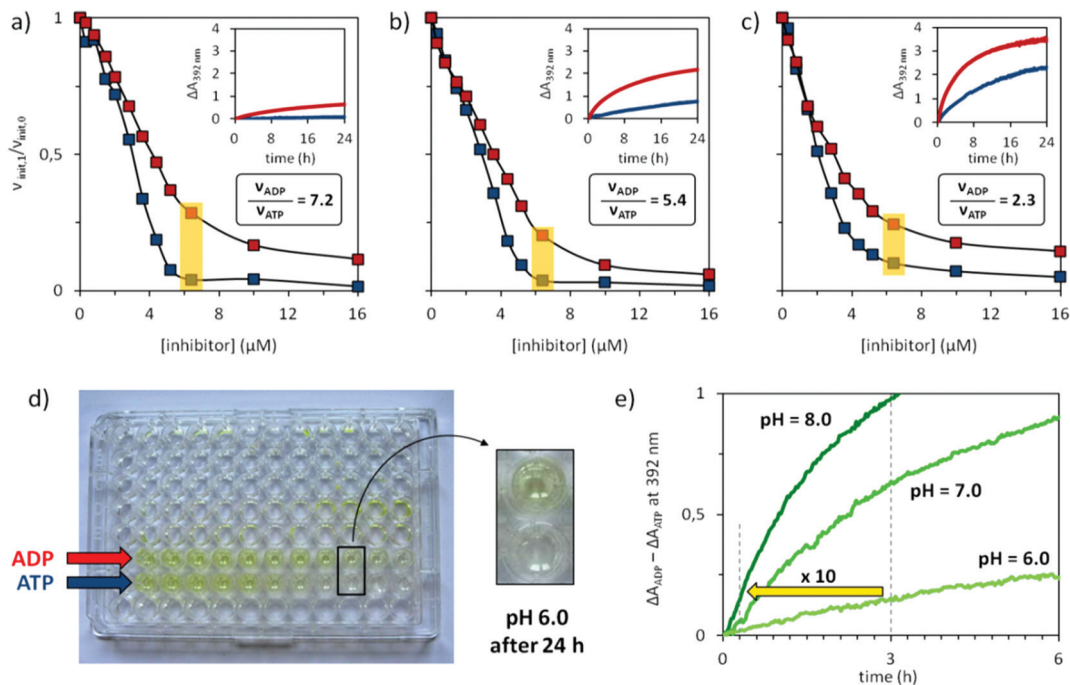


Fig. 5 Inhibition curves of ATP (blue) and ADP (red) at pH 6.0 (a), pH 7.0 (b) and pH 8.0 (c). The time course of ΔA corresponding to the concentration at which the difference between ATP (blue) and ADP (red) is maximized ($6.4 \mu\text{M}$) is reported in the inset. (d) Representative inhibition experiment at pH 6.0. The zoom indicates the wells containing $6.4 \mu\text{M}$ of ADP (top) or ATP (bottom) after 24 h at pH 6.0. (e) Signal amplification at the three different pHs in the presence of $6.4 \mu\text{M}$ of inhibitors (see ESI† for the full kinetics). Experimental conditions: $[\text{TACN}\cdot\text{Zn}^{2+}] = 20 \mu\text{M}$, $[\text{S}] = 1 \text{ mM}$, $[\text{HEPES}] = 10 \text{ mM}$, $\text{pH} = 8.0$ or 7.0 , $[\text{MES}] = 10 \text{ mM}$, $\text{pH} 6.0$, $[\text{ATP or ADP}] = 0\text{--}16 \mu\text{M}$, 40°C .

the differentiation power) was observed to be greatest at pH 6.0 ($\nu_{\text{ADP}}/\nu_{\text{ATP}} = 7.2$), where the K_{M} of 5 has its minimum (0.11 mM), while the poorest differentiation was observed at pH 8.0 ($\nu_{\text{ADP}}/\nu_{\text{ATP}} = 2.3$). However, it is important to remember that the efficacy of the assay for discriminating between ATP and ADP is determined by the absolute change in output signal, which depends not only on the discriminatory value, but also on the reaction rate and the molar extinction coefficient at a given pH. Interestingly, the analysis of the difference in output signal for ATP and ADP (expressed by $\Delta A_{\text{ADP}} - \Delta A_{\text{ATP}}$) demonstrates that in this case the combination of a faster reaction rate and a stronger output signal at higher pH more than compensates for the lower discriminatory power. For example, the same level of amplification obtained after 3.0 h at pH 6.0 ($\Delta\Delta A \approx 0.14$) is reached almost 10 times faster (after *ca.* 20 min) at pH 8.0 (Fig. 5e). This response curve also demonstrates a key attractive feature of catalytic signal amplification, which is the increase in signal intensity as a function of time. The ability of the assay to convert the difference in ATP and ADP at $6.4 \mu\text{M}$ into a difference in absorbance of over 0.14 units in just 20 minutes demonstrates the sensitivity of the assay. Fig. 5d also illustrates the ease by which the presence of ADP or ATP can be easily visually distinguished, as well as the potential use of this methodology for high-throughput screening.

To demonstrate the potential of the described gold nanoparticle system to detect the enzymatic consumption of ATP in

a practical setting, the enzyme alkaline phosphatase was chosen. An assay was set up whereby all components of the system were first pipetted into wells in a 96-well microtitre plate and allowed to stabilise for 30 min to demonstrate the lack of signal in the absence of added enzyme (Fig. 6). After 30 min, the enzyme alkaline phosphatase was added *in situ*

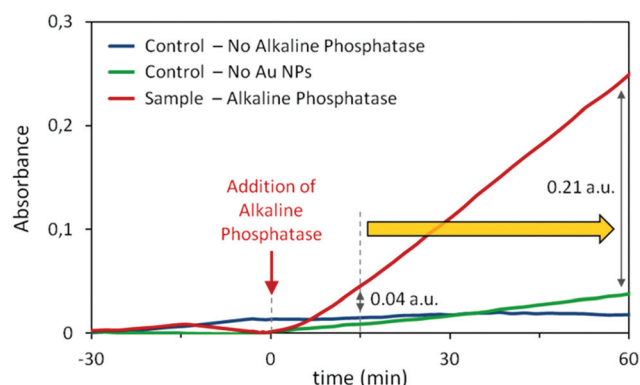


Fig. 6 The use of the above described gold nanoparticle system for the *in situ* detection of alkaline phosphatase activity. The increase in signal over time demonstrates the utility and advantage of using catalytic signal amplification for signal generation. Experimental conditions: $[\text{TACN}\cdot\text{Zn}^{2+}] = 20 \mu\text{M}$, $[\text{S}] = 1 \text{ mM}$, $[\text{HEPES}] = 10 \text{ mM}$, $\text{pH} = 7.0$, $[\text{ATP}] = 6.4 \mu\text{M}$, 40°C , $[\text{alkaline phosphatase}] = 3.3 \text{ U mL}^{-1}$.

into the microtitre plate (Fig. 6, see sample – alkaline phosphatase). It can be observed that there is significant increase in the absorbance intensity at 392 nm only for the sample of interest. Controls were performed both in the absence of alkaline phosphatase, and in the presence of alkaline phosphatase but without of Au NPs, to show that both the Au NP catalytic system and the enzyme alkaline phosphatase need to be present for a signal to be observed. The advantage of using catalytic signal amplification for the generation of a signal in an assay is clearly seen in Fig. 6. A signal difference of 0.04 absorbance units after 15 min is translated to a difference of 0.21 absorbance units at 60 min. This generation of signal by catalytic amplification allows the signal generated to be readily observed by the naked eye, reinforcing the practicality of this methodology. Currently we are exploring the possibility to use this assay for the detection of PK-activity.

Conclusions

In conclusion, we have shown for the first time a system able to discriminate ATP from ADP by means of catalytic signal amplification. The approach relies on the use of gold nanoparticles coated with TACN·Zn²⁺ head groups which are able to catalyze the transphosphorylation of the compound 2-hydroxypropyl-(3-trifluoromethyl-4-nitro)phenyl phosphate 5, with release of a chromogenic reporter. Phosphate 5 was found to possess faster kinetics than the more commonly employed HPNPP, and its increased affinity for the nanoparticle surface allowed for the discrimination of ATP and ADP. This methodology is conducive to high-throughput screening with results that can be easily detected, even with the naked eye. Overall, this represents a viable new approach for monitoring the consumption of ATP with very high sensitivity.

Experimental

Reagents and materials

Au NP 1 was prepared and characterised as previous described,⁴⁶ Zn(NO₃)₂ was an analytical grade reagent and the concentration was determined by atomic absorption spectroscopy. ATP, ADP, 2-(*N*-morpholino)ethanesulfonic acid (MES), 4-(2-hydroxyethyl)-1-piperazineethanesulfonic acid (HEPES), *N*-cyclohexyl-3-aminopropanesulfonic acid (CAPS) and alkaline phosphatase from bovine intestinal mucosa (P5521 SIGMA) were purchased from Sigma Aldrich and used without further purification. In all cases, stock solutions were prepared using deionized water filtered with a Milli-Q water-purifier (Millipore) and stored at 4 °C. For the syntheses of substrates, all commercially available reagents were purchased from Sigma-Aldrich and used as received. Anhydrous solvents were purchased and used without further purification. Chromatographic columns were packed with silica gel Macherey-Nagel 230–400 mesh, while TLC analyses were performed with silica gel 60-F254 plates.

Instrumentation

¹H, ¹³C and ³¹P-NMR spectra were recorded using a Bruker AV300 spectrometer operating at 75, 121 and 300 MHz for ¹³C, ³¹P and ¹H, respectively. Chemical shifts (δ) are reported in ppm using CDCl₃ or D₂O residual solvent values as internal reference. ³¹P-NMR spectra were calibrated using a solution of H₃PO₄ 80% as external standard. The coupling constants (*J*) are listed in Hertz (Hz), while the multiplicity of the signals are shown as follow: s: singlet, d: doublet, t: triplet, q: quartet, sp: septet, m: multiplet.

ESI-MS measurements were performed on an Agilent Technologies 1100 Series LC/MSD Trap-SL spectrometer equipped with an ESI source, hexapole filter and ionic trap. All the sample solutions were prepared in neutral solvents (ACN or MeOH). In all cases the mass of the anionic species were characterized operating in the negative mode.

HPLC purifications were performed on a preparative HPLC Shimadzu LC-8A equipped with a Shimadzu SPD-20A UV detector. The column used for separation was a Jupiter Proteo 4u 90A 250 × 21.20 mm, 4 μ m. All the runs were carried out using a flow of 17 mL min⁻¹. Eluents: neutral H₂O (A) and ACN (B).

The pH of buffer solutions were determined at room temperature using a Metrohm-632 pH meter equipped with a Ag/AgCl/KCl reference electrode. UV-Vis measurements were recorded on a TECAN M1000 PRO micro-plate reader using UV-Star® Greiner Bio-one microtiter plates (cycloolefin 96-WELL).

Synthesis of substrates

Synthesis of 2-[(*tert*-butyldimethylsilyloxy)ethyl-1-yl 4-nitrophenyl phosphate, TEA salt (10). In a three-necked flask, a solution of alcohol 8⁵⁹ (1.6 g, 6.3 mmol) and TEA (0.88 mL, 6.3 mmol) in anhydrous THF (20 mL) was added dropwise over a period of 30 min to a stirred solution of commercially available 4-nitrophenyldi-chlorophosphate in anhydrous THF (40 mL) cooled to 0 °C under nitrogen. After the complete addition, the mixture was stirred at R.T. for 2 hours. Finally, a mixture of TEA/cold water (3/12 mL) was added to hydrolyze the intermediate monochloridate and the solution was stirred for a further 30 minutes. THF was evaporated and the product extracted into CH₂Cl₂ and washed with H₂O and brine, dried over MgSO₄ and the organic solvent removed under reduced pressure. The product was purified by column chromatography (SiO₂, MeOH from 0 to 5%/CHCl₃ with 0.5% TEA) to give 10 as a pale yellow oil (1.34 g, 43%).

¹H-NMR (CDCl₃) δ (ppm): 8.12–8.09 (d, 2H, ³*J* = 9.1 Hz, *H_g*), 7.39–7.36 (d, 2H, ³*J* = 9.1 Hz, *H_f*), 4.37 (m, 1H, –CH–CH₂–), 3.50 (m, 2H, –CH₂–CH–), 3.00 (q, 6H, ³*J* = 7.3 Hz, –CH₂–CH₃), 1.27 (t, 9H, ³*J* = 7.3 Hz, –CH₂–CH₃), 1.22–1.20 (d, 3H, ³*J* = 6.2 Hz, –CH–CH₃), 0.81 (s, 9H, –C(CH₃)₃), –0.05 (s, 6H, –Si(CH₃)₂).

¹³C-NMR (CDCl₃) δ (ppm): 159.6 (d, 6.2 Hz), 143.1, 125.7, 120.5 (d, *J* = 5.7 Hz), 74.0 (d, *J* = 4.8 Hz), 68.0 (d, *J* = 6.7 Hz), 46.2, 26.3, 18.8 (d, *J* = 18.8 Hz), 9.2, –4.9.

³¹P-NMR (CDCl₃) δ (ppm): –8.03 (d, *J*(P,H) = 8.3 Hz).

MS-ESI (FIA,(-)-mode, ACN), *m/z*: Calcd for C₁₅H₂₅NO₇PSi⁻: 390.4; found 390.0.

Synthesis of 2-hydroxyethyl-1-yl 4-nitrophenyl phosphate, sodium salt (4). To a solution of **10** (1.03 g, 2.1 mmol) in anhydrous THF (10 mL) was added a solution of TEA·3HF complex (1.40 mL, 8.4 mmol) in THF (2 mL) at R.T. and the resulting mixture was stirred for 5 h before the addition of H₂O (15 mL) and TEA until pH ~ 5. THF was evaporated and the aqueous solution washed with Et₂O to remove *tert*-butyldimethylsilyl fluoride. After evaporation of Et₂O, the crude product was extracted several times into CH₂Cl₂, washed with H₂O to remove undesired triethylammonium salts and passed through an ion exchange resin (Sephadex C-50, Na⁺). The water was removed by rotary evaporation. EtOH was added and undissolved inorganic salts were removed by filtration. EtOH was removed under reduced pressure furnishing the desired product **4** as a white solid (157 mg, 25%).

¹H-NMR (D₂O), δ (ppm): 8.33–8.30 (d, 2H, ³J = 9.2 Hz, H_e), 7.43–7.40 (d, 2H, ³J = 9.1 Hz, H_d), 4.49 (m, 1H, -CH-CH₂-), 3.66 (m, 2H, -CH-CH₂), 1.32–1.30 (d, 3H, ³J = 6.4 Hz, -CH-CH₃).

¹³C-NMR (D₂O) δ (ppm): 158.0 (d, 6.4 Hz), 143.8, 126.3, 120.9, 75.3–75.2 (m), 65.8–65.7 (d, J = 8.2 Hz), 17.5.

³¹P-NMR (D₂O), δ (ppm): -4.64 (d, J(P,H) = 7.7 Hz).

MS-ESI (FIA,(-)-mode, ACN), *m/z*: Calcd for C₉H₁₁NO₇P⁻: 276.2, found: 275.8.

The synthesis of 2-hydroxypropyl 3-trifluoromethyl-4-nitrophenyl phosphate, sodium salt (**5**) was performed according to our previously described procedure.⁵⁸

Synthesis of 4-methylumbelliferyl phosphodichloridate (7c). In a dry 3-necked flask equipped with a condenser, commercially available 4-methylumbelliferone (1.5 g, 8.5 mmol) was suspended in anhydrous toluene (50 mL) and freshly distilled POCl₃ (1.82 mL, 19.6 mmol) was added. The reaction mixture was heated to 95 °C and pyridine (680 μL) was added by syringe pump over a period of 30 min. The reaction was heated at reflux (110 °C) for a further 15 min after the addition was completed and the salts were removed by filtration of the cooled reaction mixture. The obtained filtrated solution (green) was concentrated under reduced pressure and the resulting purple oil was used in the next steps without further purification.

¹H-NMR (CDCl₃), δ (ppm): 7.80 (dd, 1H, ³J = 8.7, 2.4 Hz, H_c), 7.33–7.25 (m, 2H, H_d, H_e), 6.32 (s, 1H, H_a), 2.51–2.50 (d, J = 23 Hz, 3H, H_b).

³¹P-NMR (CDCl₃), δ (ppm): 4.27 (s).

Synthesis of 2-[(*tert*-butyldimethylsilyloxy)propyl 4-methylumbelliferyl phosphate, TEA salt (11c). Phosphodichloridate **7c** (5.7 mmol) was dissolved in anhydrous THF (30 mL), and cooled to 0 °C under nitrogen. A solution of alcohol **9**⁶⁰ (1.08 g, 5.7 mmol) and TEA (0.79 mL, 5.7 mmol) in anhydrous THF (20 mL) was added dropwise over a period of 30 min. After addition was complete, the mixture was allowed to stir at R.T. for 5 h. Finally, a mixture of TEA/cold water (2/14 mL) was added to hydrolyze the intermediate monochloridate and the solution was stirred for a further 30 minutes. THF was evaporated

and the product extracted into CH₂Cl₂ and washed with H₂O and brine, dried over MgSO₄ and the organic solvent removed under reduced pressure. The product was purified by gravimetric column chromatography (SiO₂, MeOH from 0 to 5%/CHCl₃ with 0.5% TEA) to afford the TEA salt of **11c** (2.18 g, 90%).

¹H-NMR (CDCl₃), δ (ppm): 7.47–7.44 (d, 1H, ³J = 9.3 Hz, H_f), 7.26 (d, 2H, ³J = 0.5 Hz, H_d, H_e), 6.13 (s, 1H, H_h), 3.92–3.67 (m, 2H + 1H, -CH-CH₂-), 3.02–2.94 (q, 6H, ³J = 7.2 Hz, -CH₂-CH₃), 2.38 (s), 1.30–1.25 (t, 9H, ³J = 7.2 Hz, -CH₂-CH₃), 1.11–1.09 (d, 3H, ³J = 5, 9 Hz, -CH-CH₃), 0.82 (s, 9H, -C-(CH₃)₃), 0.00 (s, 6H, -Si-(CH₃)₂).

¹³C-NMR (CDCl₃), δ (ppm): 161.2 (d, J = 5.6 Hz), 156.6, 154.4, 152.5, 125.0, 116.7, 114.9, 112.5 (d, J = 9.4 Hz), 107.8, 71.0, 67.6, 45.6, 25.7, 20.6, 18.3, 8.7, -4.9.

³¹P-NMR (CDCl₃), δ (ppm): -4.39 (t, ³J(P,H) = 6.1 Hz).

MS-ESI (FIA,(-)-mode, ACN), *m/z*: calcd for C₁₉H₂₈O₇PSi⁻: 427.5; found 427.0.

Synthesis of 2-hydroxypropyl 4-methylumbelliferyl phosphate, sodium salt (6). To a solution of **11c** (1.22 g, 2.85 mmol) in anhydrous THF (10 mL) was added a solution of TEA·3HF complex (1.86 mL, 11.4 mmol) in anhydrous THF (2 mL) at R.T. The resulting pale yellow mixture was stirred until the disappearance of **11c** (followed by ESI-MS⁺), before the addition of H₂O (15 mL) and TEA until pH ~ 6.5. THF and the resulting volatile *tert*-butyldimethylsilyl fluoride were removed by rotary evaporation. The crude product was then extracted several times into CH₂Cl₂ (3 × 25 mL), washed with H₂O to remove undesired triethylammonium salts and passed through an ion exchange resin (Sephadex C-50, Na⁺). The water was removed by rotary evaporation. EtOH was added and undissolved inorganic salts were removed by filtration. EtOH was removed under reduced pressure furnishing 250 mg of the desired product **6** as a white solid (26%).

¹H-NMR (D₂O), δ (ppm): 7.70–7.67 (d, 1H, ³J = 8.6 Hz, H_f), 7.23–7.15 (dd, 2H, ³J = 13.4 Hz, ⁴J = 2.22 Hz, H_d, H_e), 6.22 (s, 1H, H_h), 4.10–3.86 (m, 2H + 1H, -CH-CH₂-), 2.41 (s, 3H, -CH₃), 1.23–1.21 (d, 3H, -CH-CH₃).

¹³C-NMR (D₂O), δ (ppm): 164.3, 156.0, 154.9 (d, J = 6.5 Hz), 153.4, 126.5, 117.3 (d, J = 4.8 Hz), 116.2, 111.8, 107.9 (d, J = 5.2 Hz), 70.0 (d, J = 6.3 Hz), 66.6 (d, J = 8.2 Hz), 17.8 (d, J = 14.9 Hz).

³¹P-NMR (D₂O), δ (ppm): -3.74 (t, J = 9.5 Hz).

MS-ESI (FIA,(-)-mode, ACN), *m/z*: Calcd for C₁₃H₁₄O₇P⁻: 313.2, found: 312.9.

UV-vis measurements

Calibration curves. The calibration curves were carried out at 40 °C by measuring the absorbance at 400 or 392 nm of increasing amounts of **3a**, **3b** or **3c** (final concentration: from 0 to 100 μM) added to a aqueous solution (buffered at the desired pH, [buffer] = 10 mM) containing Au NP 1·Zn²⁺ (20 μM) (V_{well} = 250 μL). Taking into account the Lambert-Beer law, the slope of the curve represents ε·l. The obtained values are listed in the table below and were used to convert initial

rates (ν_{init}) from dA/dt , to dC/dt . See ESI† for full UV-vis spectra and interpolations.

List of all the $\epsilon \cdot l$ values used (M^{-1})

| Leaving group | λ (nm) | pH 6.0 | pH 7.0 | pH 8.0 | pH 11.0 |
|---------------|----------------|--------|--------|--------|---------|
| 3a | 400 | 1378 | 5820 | 10 087 | 12 966 |
| 3b | 392 | 3277 | 7394 | 8471 | 9745 |
| 3c | 360 | 516 | 2194 | 6516 | 13 102 |

Hydrolysis of the substrates. The hydrolysis was carried out by monitoring the absorbance of the corresponding leaving group in an aqueous solution ([CAPS] = 10 mM, pH = 11.0) containing the substrate (2, 4, 5, or 6) at a final concentration of 50 μM ($V_{\text{well}} = 250 \mu\text{L}$, 40 °C). In order to avoid volume changes during the analysis, a transparent plastic strip on the top of the wells was applied before the measurement. The obtained profiles were nicely fitted with a first order kinetic:

$$[\text{PNP}]_t = 1 - e^{-kt}$$

(Origin 8 Pro, function: Mn Molecular 1 $A_1 - A_2 e^{-kt}$, constraints; $A_1 = A_2 = 1$). Stock solutions of substrates were prepared by weight from the final product of synthesis. This experiment was used to determine accurately their concentration using the plateau value (full conversion) and the corresponding $\epsilon \cdot l$ listed in the above table.

Michaelis-Menten kinetics. The catalytic activity of Au NP 1·Zn²⁺ was measured by monitoring the release rate of the leaving group in different aqueous solutions (buffered at the desired pH, [buffer] = 10 mM) containing Au NP 1·Zn²⁺ (20 μM) and increasing amounts of substrate. The evolution of the absorbance at 400, 392 or 360 nm was monitored at 40 °C after adding 2, 4, 5, or 6, final concentration: from 0 to 2.0 mM ($V_{\text{well}} = 250 \mu\text{L}$). In order to avoid volume changes during the analysis, a transparent plastic strip on the top of the wells was applied immediately after the additions of the substrates. Initial rates (ν_0) were calculated converting the absorbance signals into concentration using the corresponding $\epsilon \cdot l$ listed in the above table. Michaelis-Menten parameters were extrapolated by fitting the corresponding saturation profile with the Michaelis-Menten model:

$$\nu = \frac{V_{\text{max}} \cdot [\text{Substrate}]}{K_m + [\text{Substrate}]}$$

(Origin 8 Pro, function: Hill, constraints; $n = 1$, i.e. Michaelis-Menten kinetic). k_{cat} values were obtained by dividing V_{max} to the concentration of TACN·Zn²⁺ (20 μM).

Inhibition experiments with ATP and ADP. The catalytic activity of Au NP 1·Zn²⁺ was measured by monitoring the release rate of chromophore 3b in different aqueous solutions (buffered at the desired pH, [buffer] = 10 mM) containing Au NP 1·Zn²⁺ (20 μM) and increasing amounts of ATP or ADP (final concentration = from 0 to 16 μM). The evolution of the absorbance at 392 nm was monitored at 40 °C after adding substrate 5 (final concentration = 1 mM). In order to avoid

volume changes during the analysis, a transparent plastic strip on the top of the wells was applied immediately after the additions of the substrate. Initial rates were scaled to the initial rate observed in the absence of inhibitor (i.e. $\nu_{\text{init},1}/\nu_{\text{init},0}$). The kinetics at which the differentiation is maximized (6.4 μM of inhibitors) were obtained using a well-volume of 50 μL . A shorter optical path length was needed to avoid saturation of the detector.

Catalytic signal amplification with alkaline phosphatase. The catalytic activity of Au NP 1·Zn²⁺ in the presence and absence of alkaline phosphatase was measured by monitoring the release rate of chromophore 3b in buffer at pH 7 (HEPES = 10 mM) containing Au NP 1·Zn²⁺ (20 μM) and 6.4 μM of ATP. The evolution of the absorbance at 392 nm was monitored at 40 °C after adding substrate 5 (final concentration = 1 mM). In Fig. 6 - 'Control - no alkaline phosphatase,' the above described solution was observed over time to determine the background signal. For 'Control - No Au NPs,' the above described solution, but without Au NP 1 was incubated for 30 min before the addition alkaline phosphatase at $t = 0$. For 'Sample - Alkaline Phosphatase,' the above described solution was incubated for 30 min before the addition of alkaline phosphatase at $t = 0$.

Acknowledgements

Financial support from the ERC (StG-239898), University of Padova (CPDA138148) and COST (CM1304) is acknowledged.

Notes and references

- 1 S. Naylor, *Expert Rev. Mol. Diagn.*, 2003, **3**, 525–529.
- 2 F. P. Perera and I. B. Weinstein, *Carcinogenesis*, 2000, **21**, 517–524.
- 3 D. Diamond, *Principles of Chemical and Biological Sensors*, Wiley, New York, 1998.
- 4 P. Scrimin and L. J. Prins, *Chem. Soc. Rev.*, 2011, **40**, 4488–4505.
- 5 T. Pawson and J. D. Scott, *Trends Biochem. Sci.*, 2005, **30**, 286–290.
- 6 S. A. Johnson and T. Hunter, *Nat. Methods*, 2005, **2**, 17–25.
- 7 M. B. Yaffe, *Nat. Rev. Mol. Cell Biol.*, 2002, **3**, 177–186.
- 8 L. N. Johnson and R. J. Lewis, *Chem. Rev.*, 2001, **101**, 2209–2242.
- 9 C. J. Hastie, H. J. McLauchlan and P. Cohen, *Nat. Protoc.*, 2006, **1**, 968–971.
- 10 H. C. Ma, S. Deacon and K. Horiuchi, *Expert Opin. Drug Discovery*, 2008, **3**, 607–621.
- 11 N. P. Oien, L. T. Nguyen, F. E. Jernigan, M. A. Priestman and D. S. Lawrence, *Angew. Chem., Int. Ed.*, 2014, **53**, 3975–3978.
- 12 Y. J. Li, W. H. Xie and G. J. Fang, *Anal. Bioanal. Chem.*, 2008, **390**, 2049–2057.
- 13 B. E. Turk, *Nat. Methods*, 2005, **2**, 251–252.

- 14 K. Kupcho, R. Somberg, B. Bulleit and S. A. Goueli, *Anal. Biochem.*, 2003, **317**, 210–217.
- 15 E. A. Gaudet, K. S. Huang, Y. Zhang, W. Huang, D. Mark and J. R. Sportsman, *J. Biomol. Screening*, 2003, **8**, 164–175.
- 16 F. S. Wouters and P. I. H. Bastiaens, *Curr. Biol.*, 1999, **9**, 1127–1130.
- 17 T. Noguchi, B. Roy, D. Yoshihara, Y. Tsuchiya, T. Yamamoto and S. Shinkai, *Chem. Sci.*, 2015, **6**, 3863–3867.
- 18 C. Pezzato, D. Zaramella, M. Martinelli, G. Pieters, M. A. Pagano and L. J. Prins, *Org. Biomol. Chem.*, 2015, **13**, 1198–1203.
- 19 X. Liu, Y. Li, X. H. Xu, P. Li, Z. Nie, Y. Huang and S. Z. Yao, *Trends Anal. Chem.*, 2014, **58**, 40–53.
- 20 J. Bai, C. H. Liu, T. Yang, F. F. Wang and Z. P. Li, *Chem. Commun.*, 2013, **49**, 3887–3889.
- 21 S. Martic and H. B. Kraatz, *Chem. Sci.*, 2013, **4**, 42–59.
- 22 G. Ghale, V. Ramalingam, A. R. Urbach and W. M. Nau, *J. Am. Chem. Soc.*, 2011, **133**, 7528–7535.
- 23 A. E. Hargrove, S. Nieto, T. Z. Zhang, J. L. Sessler and E. V. Anslyn, *Chem. Rev.*, 2011, **111**, 6603–6782.
- 24 T. Z. Zhang, N. Y. Edwards, M. Bonizzoni and E. V. Anslyn, *J. Am. Chem. Soc.*, 2009, **131**, 11976–11984.
- 25 L. Zhu and E. V. Anslyn, *Angew. Chem., Int. Ed.*, 2006, **45**, 1190–1196.
- 26 W. Bai, N. A. Gariano and D. A. Spivak, *J. Am. Chem. Soc.*, 2013, **135**, 6977–6984.
- 27 E. Sella and D. Shabat, *J. Am. Chem. Soc.*, 2009, **131**, 9934–9936.
- 28 N. C. Gianneschi, S. T. Nguyen and C. A. Mirkin, *J. Am. Chem. Soc.*, 2005, **127**, 1644–1645.
- 29 G. Das, P. Talukdar and S. Matile, *Science*, 2002, **298**, 1600–1602.
- 30 R. Bonomi, A. Cazzolaro, A. Sansone, P. Scrimin and L. J. Prins, *Angew. Chem., Int. Ed.*, 2011, **50**, 2307–2312.
- 31 F. Manea, F. B. Houillon, L. Pasquato and P. Scrimin, *Angew. Chem., Int. Ed.*, 2004, **43**, 6165–6169.
- 32 E. Y. Tirel, Z. Bellamy, H. Adams, V. Lebrun, F. Duarte and N. H. Williams, *Angew. Chem., Int. Ed.*, 2014, **53**, 8246–8250.
- 33 F. Mancin, P. Scrimin and P. Tecilla, *Chem. Commun.*, 2012, **48**, 5545–5559.
- 34 R. Bonomi, F. Selvestrel, V. Lombardo, C. Sissi, S. Polizzi, F. Mancin, U. Tonellato and P. Scrimin, *J. Am. Chem. Soc.*, 2008, **130**, 15744–15745.
- 35 A. A. Neverov, Z. L. Lu, C. I. Maxwell, M. F. Mohamed, C. J. White, J. S. W. Tsang and R. S. Brown, *J. Am. Chem. Soc.*, 2006, **128**, 16398–16405.
- 36 N. H. Williams, B. Takasaki, M. Wall and J. Chin, *Acc. Chem. Res.*, 1999, **32**, 485–493.
- 37 J. Chin, *Curr. Opin. Chem. Biol.*, 1997, **1**, 514–521.
- 38 W. H. Chapman and R. Breslow, *J. Am. Chem. Soc.*, 1995, **117**, 5462–5469.
- 39 G. Zaupa, C. Mora, R. Bonomi, L. J. Prins and P. Scrimin, *Chem. – Eur. J.*, 2011, **17**, 4879–4889.
- 40 G. Zaupa, P. Scrimin and L. J. Prins, *J. Am. Chem. Soc.*, 2008, **130**, 5699–5709.
- 41 C. Pezzato, P. Scrimin and L. J. Prins, *Angew. Chem., Int. Ed.*, 2014, **53**, 2104–2109.
- 42 C. Pezzato, B. Lee, K. Severin and L. J. Prins, *Chem. Commun.*, 2013, **49**, 469–471.
- 43 A. Ojida, K. Honda, D. Shinmi, S. Kiyonaka, Y. Mori and I. Hamachi, *J. Am. Chem. Soc.*, 2006, **128**, 10452–10459.
- 44 A. Ojida, M. Inoue, Y. Mito-oka, H. Tsutsumi, K. Sada and I. Hamachi, *J. Am. Chem. Soc.*, 2006, **128**, 2052–2058.
- 45 A. Ojida, Y. Mito-oka, K. Sada and I. Hamachi, *J. Am. Chem. Soc.*, 2004, **126**, 2454–2463.
- 46 G. Pieters, A. Cazzolaro, R. Bonomi and L. J. Prins, *Chem. Commun.*, 2012, **48**, 1916–1918.
- 47 B. Perrone, S. Springhetti, F. Ramadori, F. Rastrelli and F. Mancin, *J. Am. Chem. Soc.*, 2013, **135**, 11768–11771.
- 48 G. Pieters, C. Pezzato and L. J. Prins, *Langmuir*, 2013, **29**, 7180–7185.
- 49 D. Zaramella, P. Scrimin and L. J. Prins, *J. Am. Chem. Soc.*, 2012, **134**, 8396–8399.
- 50 X. Liu, Y. Hu and F. Stellacci, *Small*, 2011, **7**, 1961–1966.
- 51 R. L. Phillips, O. R. Miranda, D. E. Mortenson, C. Subramani, V. M. Rotello and U. H. F. Bunz, *Soft Matter*, 2009, **5**, 607–612.
- 52 G. V. Oshovsky, D. N. Reinhoudt and W. Verboom, *Angew. Chem., Int. Ed.*, 2007, **46**, 2366–2393.
- 53 A. V. Ellis, K. Vjayamohan, R. Goswami, N. Chakrapani, L. S. Ramanathan, P. M. Ajayan and G. Ramanath, *Nano Lett.*, 2003, **3**, 279–282.
- 54 B. G. Tehan, E. J. Lloyd, M. G. Wong, W. R. Pitt, E. Gancia and D. T. Manallack, *Quant. Struct.-Act. Rel.*, 2002, **21**, 473–485.
- 55 R. Strachan, J. Wood and R. Hirschmann, *J. Org. Chem.*, 1962, **27**, 1074–1075.
- 56 T. Humphry, S. Iyer, O. Iranzo, J. R. Morrow, J. P. Richard, P. Paneth and A. C. Hengge, *J. Am. Chem. Soc.*, 2008, **130**, 17858–17866.
- 57 J. P. Horwitz and J. V. Freisler, *J. Med. Chem.*, 1970, **13**, 1024–1025.
- 58 J. L.-Y. Chen, C. Pezzato, P. Scrimin and L. J. Prins, *Chem. – Eur. J.*, 2016, **22**, 7028–7032.
- 59 R. S. Perali, S. Mandava and V. R. Chunduri, *Tetrahedron Lett.*, 2011, **52**, 3045–3047.
- 60 R. A. Pilli, M. M. Victor and A. de Meijere, *J. Org. Chem.*, 2000, **65**, 5910–5916.